Received: 2 September 2024 | Revised: 24 October 2024 | Accepted: 3 November 2024

DOI: 10.1002/jex2.70023

RESEARCH ARTICLE

Hepatocyte-derived extracellular vesicles regulate liver regeneration through a negative feedback mechanism

Mina McGinn | **Christopher Rabender** | **Ross Mikkelsen** | **Vasily Yakovlev**

Department of Radiation Oncology, Massey Comprehensive Cancer Center, Virginia Commonwealth University, Richmond, Virginia, USA

Correspondence
Vasily Yakovlev, Department of Radiation Oncology, Massey Comprehensive Cancer Center, Virginia Commonwealth University, Richmond, VA, USA.
Email: vasily.yakovlev@vcuhealth.org

Funding information
NIH-NCI Cancer Center Support Grant, Grant/Award Number: P30 CA016059

Abstract

While significant progress has been made in understanding various aspects of liver regeneration, the molecular mechanisms responsible for the initiation and termination of cell proliferation in the liver following massive tissue loss or injury of liver remain unknown. As it was previously shown, the loss of liver mass affects putative hepatocyte-specific mitogenic inhibitors in the blood. Although the presence of these putative inhibitors regulating precise liver regeneration has been described in numerous publications, they have never been identified. Extracellular vesicles (EVs) are nano-sized, membrane-limited structures secreted by cells into the extracellular space. Their proposed role is stable intercellular carriers of proteins and RNAs, predominantly micro-RNA, from secreted to recipient cells. Upon uptake by the recipient cells, EVs can significantly modulate their biological functions. In the present study, using in vivo and in vitro models, we demonstrate that hepatocyte proliferation and liver regeneration are regulated by EVs secreted by hepatocytes into the bloodstream. This regulation occurs through a negative feedback mechanism, which explains the precise regeneration of liver tissue after massive damage. We also demonstrate that an essential component of this mechanism is RNA carried by hepatocyte-derived EVs. Our findings open up a new and unexplored area of liver biology regarding the mechanisms involved in the precise regulation of liver regeneration after a massive tissue loss or injury. Further study of this mechanism will have a great influence on the development of new approaches to liver transplantation, various liver pathologies, and hepatic tumors.

KEYWORDS

AML-12, extracellular vesicles, hepatocyte, liver injury, liver regeneration, partial hepatectomy

1 | INTRODUCTION

The liver is known for its remarkable ability to regenerate precisely after massive tissue loss or injury (Michalopoulos & DeFrances, 1997). Liver regeneration is studied by performing the partial hepatectomy (PHx) to remove 2/3 of the liver mass in rodents (rats and mice) (Fausto et al., 2006; Michalopoulos & Bhushan, 2021; Mitchell & Willenbring, 2008). Following regeneration, the liver grows back precisely to its original mass without exceeding it (Apte et al., 2009; Starzl et al., 1993). Different studies have shown that loss of liver mass affects putative tissue-specific mitogenic inhibitors in the blood, which, in turn, regulate the proliferation of remaining hepatocytes and liver regeneration (Jirtle & Michalopoulos, 1982; Leong et al., 1964; Moolten & Bucher, 1967). Although well-documented in numerous publications, the inhibitory substances or 'sensor molecules' that control the regeneration mechanisms to properly maintain liver size remain unknown. Approximately 80 years ago a series of now

classic studies were published, suggesting that within any cell line, the functionally active differentiated cells may signal their existence to the mitotically active precursor cells through a tissue-specific or a cell-line-specific inhibitory substance (Bullough, 1962; Bullough & Laurence, 1960; Laird, 1965; Weiss & Kavanau, 1957). The application of this negative feedback concept to the autoregulation of cell proliferation and tissue regeneration was very appealing. The principal characteristics of these inhibitory substances were later postulated (Bullough & Laurence, 1968; Elgjo & Hennings; 1971; Iversen, 1968; Laurence & Elgjo, 1971; Marrs & Voorhees, 1971; Maugh, 1972; Nome, 1975): (a) they inhibit mitosis both in vitro and in vivo; (b) their action is reversible, and they are not cytotoxic; (c) they are synthesized by mature cells of the tissue upon which they act, released from cells and circulate in the blood stream and in humoral fluids; and (d) they are tissue-specific, but species-unspecific. In the present study, using both in vivo and in vitro models, we demonstrate that hepatocyte proliferation and liver regeneration are regulated by extracellular vesicles (EVs) secreted by hepatocytes into the bloodstream. This regulation occurs through a negative feedback mechanism, and an essential component of this mechanism is RNA transported by hepatocyte-derived EVs (HD-EVs). These findings open up an unexplored area of biology regarding the mechanisms involved in the homeostasis regulation of various constantly renewing tissues by maintaining the optimal size and correct ratio between differentiating and proliferating cells.

2 | METHODS SUMMARY

2.1 | EV isolation from plasma

EVs were extracted from plasma samples by size exclusion chromatography (SEC) method using the qEV columns (Izon Science, Christchurch, New Zealand) as described earlier (Rodrigues et al., 2021). Prior to EV isolation, SEC columns were conditioned by washing with freshly filtered (0.1 μm) phosphate-buffered saline (PBS). Thawed plasma was filtered (0.2 μm), added to the sample reservoir, and EVs were eluted in PBS, which was added to the sample reservoir as the last of the serum entered the column. During EV isolation, the volume of PBS in the reservoir was kept below 2 mL. The initial fractions (void volume) of flow-through were discarded, and EVs were collected as pooled fractions 1–4 (20 mL total) (Figure 2a,b). Protein fractions of plasma were also collected as pooled fractions 8–11 (20 mL total) and stored at −20°C. The resulting pooled EV fractions were mixed by gentle inversion 10 times and concentrated using preconditioned Pierce Protein Concentrator PES (100 kDa MWCO, Thermo Fisher Scientific, Waltham, MA, USA) to a final EV concentration of $2–3 \times 10^{12}$ particles/mL of PBS. EVs samples were then stored at −20°C until thawed, analyzed, and used for cell treatment and animal injection. After thawing, protein-fractions and EVs-fractions of plasma were analyzed by Western blot analysis (Figure 2c). Freshly isolated plasma EVs were analyzed by nanoparticle tracking analysis (NTA) and transmission electron microscopy (TEM) (Figure 2d,e).

2.2 | NTA

The analysis was carried out with the support of the Microscopy Core at VCU. The concentration and size of exosomes were measured using ZetaView NTA. All samples were diluted in filtered (0.1 μm) PBS. Ideal measurement concentrations were determined by pre-testing the optimal particle per frame value (140–200 particles/frame). The manufacturer's default software settings for EVs were selected accordingly. For each measurement, three cycles were performed by scanning 11 cell positions each and capturing 80 frames per position under the following settings, Focus: autofocus; Camera sensitivity for all samples: 78; Shutter: 100; Scattering Intensity: detected automatically; Cell temperature: 25°C. After capture, the videos were analyzed by the in-built ZetaView Software 8.04.02 SP2 with specific analysis parameters: Maximum area: 1000, Minimum area: 5, Minimum brightness: 25. Hardware: embedded laser: 40 mW at 488 nm; camera: CMOS. The number of completed tracks in NTA measurements was always greater than the proposed minimum of 1000 to minimize data skewing based on single large particles.

2.3 | Animals, PHx surgery, and EVs injection

The Institutional Animal Care and Use Committee of Virginia Commonwealth University approved all mouse experiments. Male C57BL/6 mice, 8–12 weeks old, were obtained from Charles River Laboratories. Mice were housed in animal facilities under specific pathogen-free conditions, receiving humane care according to the criteria of the National Institutes of Health Guide for the Care and Use of Laboratory Animals. Mice were maintained on a 12-h dark–light cycle and allowed free access to standard food and water. All experiments were conducted during the light phase. The two-thirds PHx was described previously (Mitchell & Willenbring, 2008). Livers were harvested 36–48 h after PHx (time-period with the maximum number of hepatocyte mitotic structures), 5 days after PHx, and 10 days after PHx (a time point when the level of the hepatocyte mitotic activity in the regenerated liver returns to normal).

2.4 | EV labeling, IVIS, and flow cytometry

C57BL/6 mouse plasma (Innovative Research, Novi, MI, USA) was thawed, centrifuged for 30 min at 3000 g, and submitted to microfiltration with 0.22-mm filters to remove cell debris and apoptotic bodies. Filtered plasma was then stained for 20 min at 37°C in the dark with different lipophilic carbocyanine dyes: 1 μM of DiL dye (1,1′-dioctadecyl-3,3,3′,3′-tetramethylindocarbocyanine, Thermo Fisher Scientific, Waltham, MA, USA), 1 μM DiR dye (1,1′-dioctadecyl-3,3,3′,3′-tetramethylindotricarbocyanine iodide, Thermo Fisher Scientific, Waltham, MA, USA), or 1 μM of DiB dye (CellBrite Blue Cytoplasmic Membrane Labeling Kit, Biotium, Inc., Fremont, CA, USA). Immediately after staining, EVs were extracted from plasma samples by SEC (see sub-chapter "EVs isolation from plasma" for more details) and concentrated by using preconditioned Pierce Protein Concentrator PES (100 KDa MWCO, Thermo Fisher Scientific, Waltham, MA, USA) to a final EVs concentration $2–3 \times 10^{12}$ particles/mL of PBS. The collected DiL- or DiR-stained EVs were used fresh for cell culture treatment and cell imaging (DiL-labelled EVs) or for IV injection of animals after PHx (DiR-labelled EVs). HD-EVs were labeled by overnight incubation (rotor, +4C°) with Alexa Fluor 647 (AF647)-conjugated anti-mASGR1 Ab (Bioss Antibodies, Woburn, MA, USA) at a dilution 1:500. Flow Cytometry analysis of plasma EVs labeled with DiB and AF647-conjugated anti-mASGR1 Ab was performed using the Cytek Aurora cytometer (Cytek, Bethesda, MD, USA) and analysed with SpectroFlo software. The distribution of EVs labeled with DiR ex vivo was detected using the IVIS Spectrum system (PerkinElmer, Waltham, USA) as instructed.

2.5 | Precipitation of HD-EVs

HD-EVs were selectively isolated by combining global plasma EVs (GP-EVs) with Dynabead M280 streptavidin magnetic beads (Thermo Fisher Scientific, Waltham, MA, USA) conjugated with a biotin-labeled anti-ASGPR1 polyclonal antibody (Bioss Antibodies, Woburn, MA, USA). Prior to the immunoprecipitation step, the Dynabeads (1 mg) were washed three times with 1 mL of filtered (0.1 μm) PBS, separated for 1 min using the DynaMag-2 magnet, and resuspended in 100 μL of PBS. The washed beads were then incubated with 10 μg of biotinylated anti-ASGPR1 antibody for 1 h at room temperature with gentle rotation. The antibody-coated beads were separated on the magnet for 2 min and washed four times with 500 μL of PBS containing 0.1% bovine serum albumin before resuspension in 100 μL of PBS. Isolated plasma EVs (100 μL) were then incubated with the antibody-conjugated beads (100 μL) at 4°C for 24 h on a rotating mixer. The HD-EVs (ASGPR1+ EVs) bound to Dynabeads were separated out on the magnet for 2 min and the depleted supernatant was used for extraction and concentration of non-hepatocyte EVs (NH-EVs) as was described above. As a negative control, EVs precipitation was performed with biotinylated rabbit IgG isotype control (Cell Signalling Technology, Danvers, MA, USA).

2.6 | Cell culture, cellular uptake of EVs, and heparin treatment

Normal mouse hepatocytes (AML-12) were obtained from the American Type Culture Collection and were used within 6 months after resuscitation. Cells were tested for mycoplasma contamination each 2 months. AML-12 cells were grown in a 1:1 mixture of DMEM/F-12 (Thermo Fisher Scientific, Waltham, MA, USA) supplemented with 10% EVs-depleted FBS (System Biosciences, Palo Alto, CA, USA), 40 ng/mL dexamethasone (Sigma–Aldrich, Inc., St. Louis, MO, USA), and Insulin-transferrin-sodium selenite media supplement (Sigma–Aldrich, Inc., St. Louis, MO, USA). AML-12 cells were propagated in T-75 flasks (VWR, Bridgeport, NJ, USA), and experiments were carried out in 6-well plates (Corning, Glendale, AZ, USA). Twenty-four hours after AML-12 cells were plated, the DiL-labelled EVs were added to the cell media at a final concentration of 2×10^{11} particles/mL. After incubation with labeled EVs for 1–12 h at +37°C, cells were washed with cold PBS, fixed with 4% paraformaldehyde (PFA) for 10 min at +4°C, and stained with mounting media with DAPI (Ibidi USA, Inc., Fitchburg, WI, USA) for 10 min at +25°C. To inhibit cellular uptake of EVs, cells and EVs were preincubated with 5 μg/mL heparin for 2 h. Cell images were observed using an AMG EVOS FL digital inverted microscope (Thermo Fisher Scientific, Waltham, MA, USA).

2.7 | Cell cycle analysis

For the cell cycle distribution analysis, AML-12 cells were stained with the FxCycle PI/RNase Staining Solution (Thermo Fisher Scientific, Waltham, MA, USA) following the manufacturer's instructions. Flow cytometry of the stained cells was performed with a FACSCanto II flow cytometer (BD Biosciences, Franklin Lakes, NJ, USA).

2.8 | Immunohistochemistry (IHC)

The liver samples were fixed in 10% Neutral Buffered Formalin (Sigma–Aldrich, Inc., St. Louis, MO, USA) at +4°C. Then the fixed materials were dehydrated with 70% ethanol, embedded with paraffin, and sectioned at 5 μm for staining. The IHC staining and analysis was carried out by the Tissue and Data Acquisition and Analysis Core of VCU Massey Comprehensive Cancer Center.

2.9 | Western blot analysis

For protein analysis all samples were loaded and separated by SDS-PAGE gel and transferred to nitrocellulose membranes. The membranes were exposed to antibodies at specific dilutions. Primary antibodies used for WB: anti-CD63 (dilution 1:1000, Thermo Fisher Scientific, Waltham, MA, USA), anti-TSG101 (dilution 1:500, Cell Signaling Technology, Danvers, MA, USA), anti-Albumin (dilution 1:1000, Cell Signaling Technology), anti-Cyclin D1 (dilution 1:1000, Cell Signaling Technology), anti-GAPDH (dilution 1:2000, Cell Signaling Technology), anti-PCNA (dilution 1:1000, Cell Signaling Technology). Specific protein bands were detected using infrared-emitting conjugated secondary antibodies: anti-rabbit DyLight 800 4X PEG Conjugate (dilution 1:10,000, Cell Signaling Technology). WB images were generated and analysed using the Odyssey CLx imaging system and iS Image Studio 5.2.5 software (Li-Cor).

2.10 | TEM of isolated EVs

Isolated EVs were fixed and prepared for the TEM as previously described (Jung & Mun, 2018; Thery et al., 2006). Briefly, purified EVs resuspended in PBS were fixed with an equal volume of 4% PFA (Thermo Fisher Scientific, Waltham, MA, USA) containing 0.1 M sodium cacodylate buffer (Avantor, Allentown, PA, USA). The final concentration of this solution is 2% PFA, and samples were kept in fixative for up to 48 h at +4°C until further processed. Eight microliter drops of each fixed sample were deposited onto a Formvar-coated grid (composed of copper with carbon) (Sigma–Aldrich, Inc., St. Louis, MO, USA) to allow the vesicles to attach to the grid for 30 min at RT. The grids were then washed with PBS and transferred onto a drop of 1% glutaraldehyde (Sigma-Aldrich, Inc., St. Louis, MO, USA) in 0.1 M sodium cacodylate buffer for 5 min. The grids were then washed with diH_2O ×5 times over the course of 2 min. After washing, grids were transferred onto a drop of fresh 0.5% aqueous uranyl acetate solution (Avantor, Allentown, PA, USA) for 3 min for staining. Grids were then blotted to remove excess liquid, air-dried (typically overnight), and stored in the dark until imaged. Following sample preparation, EVs were imaged on the JEOL JEM-1400 Plus TEM (JEOL USA, Inc., Peabody, MA, USA) with sCMOS OneView camera (Gatan, Inc., Pleasanton, CA, USA) at 100 kV. The TEM analysis was carried out with the support of the Microscopy Core of VCU.

2.11 | RNA extraction and estimation

Total RNA was purified from EV samples using the MiRNeasy Micro Kit (Qiagen) according to the manufacturer's protocol with a few modifications to maximize the recovery of small RNA from EVs. Extracted EVs (in 150 μL of PBS) were homogenized with 750 μL of TRIzol LS reagent (Invitrogen), followed by 200 μL of chloroform. Each sample was vortexed for 60 s and incubated at room temperature for 5 min. Phase separation was performed by centrifugation at 12,000×*g* for 15 min at 4°C. Three hundred μL of the upper aqueous phase were transferred to a new tube. To stimulate RNA precipitation, glycogen (5 mg/mL) (Invitrogen) was added to the aqueous phase before being mixed with 750 μL of cold 100% molecular grade Ethanol. Tubes were vortexed for 30 s and incubated at − 20°C for 1 h. After precipitation step, samples were transferred to a Qiagen RNeasy Mini spin column in a collection tube followed by centrifugation at 15,000 × *g* for 30 s at room temperature. Then, the Qiagen RNeasy Mini spin columns were washed three times according to the standard protocol. After the last wash with 70% Ethanol, the Qiagen RNeasy Mini spin columns were left uncapped for 5 min to allow the column to dry. Next, 20 μL of RNase-free pre-warmed (+65°C) water was added to the dry columns, and after 5 min of incubation, total EVs RNA was eluted in a new RNase-free collecting tubes by 1 min centrifugation at 15,000×*g*. To increase the amount of eluted RNA, columns were reloaded with the eluent and centrifuged again. The eluents with total EVs RNA were stored at −80°C. The concentration and purity of the EVs RNA were measured using NanoDrop ND-1000 spectrophotometer (Thermo Fisher Scientific, Waltham, MA, USA).

2.12 | RNA transfection in vitro and in vivo

For in vitro transfection, mouse hepatocytes (AML-12 cell line) were distributed onto 6-well plates at a concentration of 2×10^5 cells/well and incubated overnight to allow cell adherence. 24 h after plating, RNA transfection was performed in the presence of Lipofectamine RNAiMAX (Invitrogen) according to manufacturer's protocol. As a negative control, cells were transfected with *Silencer* Negative Control No. 1 siRNA (Thermo Fisher Scientific, Waltham, MA, USA). Two days after transfection, cells were trypsinized, washed, and prepared for Western blot and Cell Cycle analysis. For in vivo transfection, RNA/ Invivofectamine 3.0 Reagent (Thermo Fisher Scientific, Waltham, MA, USA) complex was prepared according to the manufacturer's protocol. Six hours after PHx, animals received tail vein injection with 200 μL volume of RNA/Invivofectamine 3.0 Reagent complex. For visualization of RNA distribution in animals' organs, and as a negative control, *Silencer* Cy3-labeled Negative Control No. 1 siRNA was used (Thermo Fisher Scientific, Waltham, MA, USA).

2.13 | Statistical significance

Statistical significance was determined using a two-sided Student's *t*-test (Figures 1c,f and 6f) or Analysis of Variance (ANOVA) (Figures 3g, 4d, 5e and 6d). *p* values less than 0.05 were considered significant.

3 | RESULTS

To assess proliferative activity in the mouse liver post-PHx, we applied the most commonly used biomarkers of cell proliferation: Cyclin D1 and PCNA. Western blotting and IHC were utilized to analyse the overall expression level and localization of biomarkers in liver tissue. We demonstrated that on the 2nd day after PHx, the period of greatest proliferative activity occurs, in which almost all hepatocytes of the remaining liver lobes were synchronically involved (Figure 1a–c). By the 10^{th} day post-PHx, when the original liver volume was restored, the expression of proliferation biomarkers and the percentage of proliferating hepatocytes had returned to levels observed in the intact (Control) animals. Next, we examined changes in the HD-EV concentration in the blood changed over the period of liver regeneration post-PHx. Asialoglycoprotein receptor 1 (ASGR1) is a well-established hepatocellular protein, and, as previously shown, can serve as a biomarker for the HD-EVs (Povero et al., 2020; Rodrigues et al., 2021). Mouse plasma EVs were isolated by the SEC method. To determine the concentration of HD-EVs in the mouse plasma, we used a double-staining method (Figure 1c). DiB, a lipophilic cationic dye, was used to stain all EVs isolated from mouse plasma, which allowed us to distinguish true EVs from other similarly-sized particles to EVs. Labeling of EVs with Alexa Fluor 647 (AF647)-conjugated anti-mASGR1 antibodies allowed identification of HD-EVs. Using the double-staining method, we demonstrated that changes in HD-EVs concentration in the blood were inversely proportional to proliferation activity in liver tissue after PHx (Figure 1d,e).

In subsequent experiments, we used EVs purified from commercially available pooled C57BL/6 mouse plasma (Innovative Research, Novi, MI, USA) by the SEC method. Ponceau S staining and NTA of various fractions after extraction of EVs from mouse plasma by SEC showed that fractions #1-4, containing the bulk of EVs, were free from contamination by plasma proteins (Figure 2a,b). Equal amounts of total protein from pooled EV fractions (fractions #1-4) and plasma protein fractions (fractions 8–11) were analysed by Western blot (Figure 2c). The absence of specific EV markers (CD9, CD63, and TSG101) in the pooled protein fractions and lack of albumin (the most abandoned plasma protein) in the pooled EVs fractions demonstrates an efficient separation of EVs from plasma proteins. This method enabled recovery of >97% of purified EVs from mouse plasma. The average plasma concentration of EVs in intact healthy mice is $2–4 \times 10^{11}$/mL (Figure 2e). In our experiments, in order to achieve an adequate response, we introduced purified EVs into the cell culture medium or mouse blood at concentrations approximating those in the plasma of the intact, healthy mice. Therefore, the purified exosomes were pre-concentrated before use (Figure 2e). TEM analysis demonstrated that the concentration step did not alter the size, shape, and integrity of EVs (Figure 2d).

Our subsequent experiments assessed the uptake of hepatocyte-derived and non-hepatocyte-derived EVs uptake by mouse hepatocytes (AML-12 cell line) in vitro (Figure 3a). We generated the HD-EV-depleted fraction of total plasma EVs (ASGR1-negEVs) by immunoprecipitation of HD-EVs with anti-ASGR1 Ab (Figure 3b). Incubation of normal mouse hepatocytes (AML-12) with DiL-stained non-hepatocyte (ASGR1-neg) EVs (NH-EVs) and global plasma EVs (GP-EVs) demonstrated that AML-12 cells exhibited significantly higher uptake of GP-EVs, which contain both HD-EVs and NH-EVs, compared to NH-EVs alone (Figure 3c). Thus, hepatocytes more actively uptake HD-EVs than EVs from other sources. Incubation of AML-12 cells with GP-EVs resulted in a dose-dependent inhibition of the cell cycle, with accumulation of cells in the G1 phase (Figure 3d,e), and reduction in expression of the proliferation biomarkers PNCA and Cyclin D1 (Figure 3f,g). It has been previously demonstrated that Heparin blocks EVs' cellular uptake. Our preliminary study also showed a dose-dependent inhibition of GP-EVs' uptake by AML-12 cells treated with heparin (Supplemental data, Figure S1). We determined that the optimal regimen for heparin involves

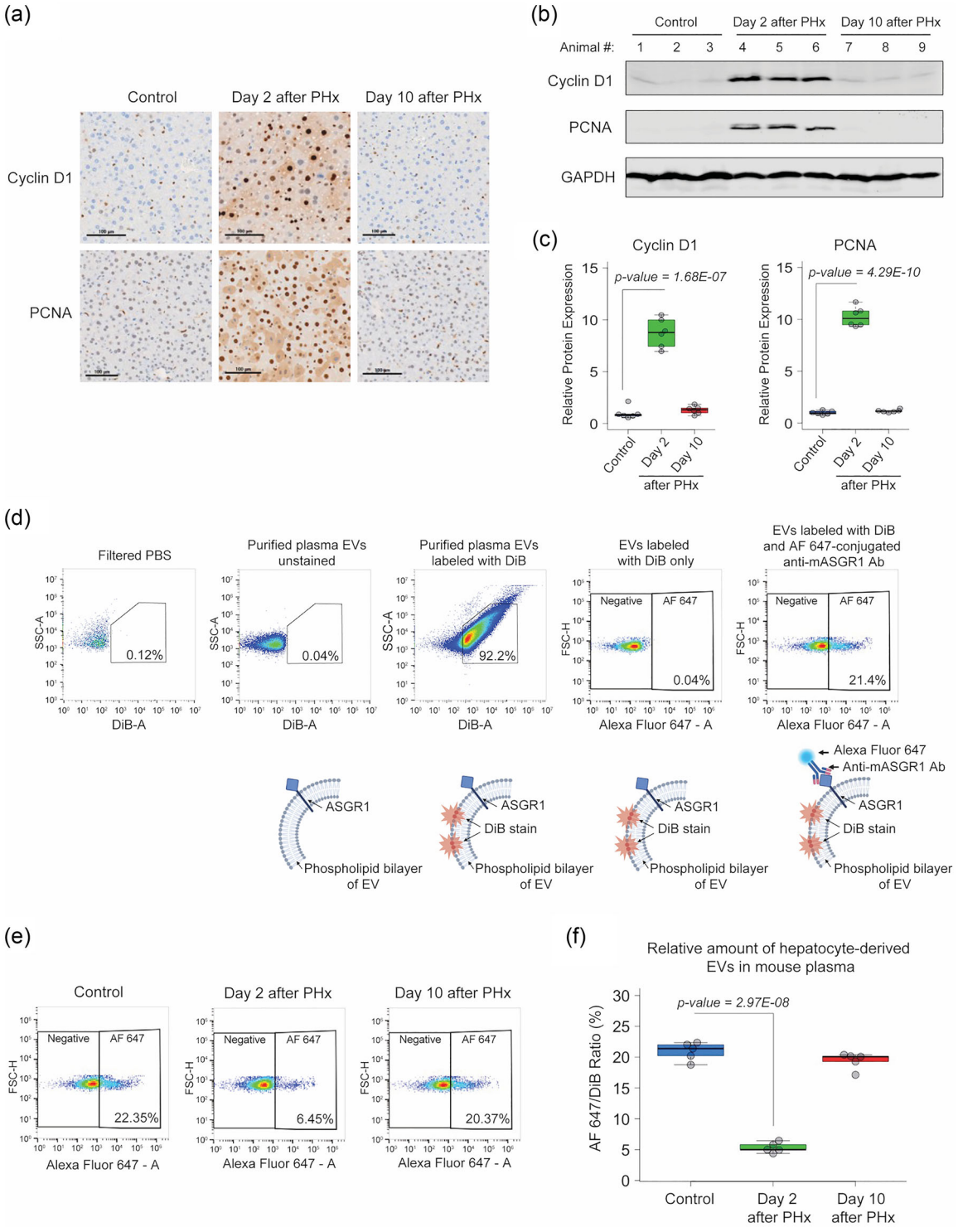

FIGURE 1 PHx affects liver hepatocyte proliferation and concentration of HD-EVs in mouse plasma. (a) IHC for proliferation markers PCNA and Cyclin D1 in liver tissue of non-surgery control mice and at the different time-points after PHx. Scale bar = 100 μm. (b) Western blot analysis of liver tissue lysates with Cyclin D1, PCNA, and GAPDH for different time-points after PHx and non-surgery control (set 1, $n = 3$ for each group). (c) Graph with quantification of the Western blot analysis as shown in (b) (two sets, $n = 6$ for each group). (d) Flow cytometry analysis of HD-EVs labeled with DiB and AF647-conjugated Anti-mASGR1 Ab and schematic representation of EVs labeling. (e) Flow cytometry analysis of HD-EVs concentration in plasma of non-surgery control animals and in the different time-points after PHx. (f) Graph with quantification of the flow cytometry analysis as shown in (e). $n = 5$ animals for each group. EVs, extracellular vesicles; HD-EVs, hepatocyte-derived EVs; IHC, immunohistochemistry; PHx, partial hepatectomy.

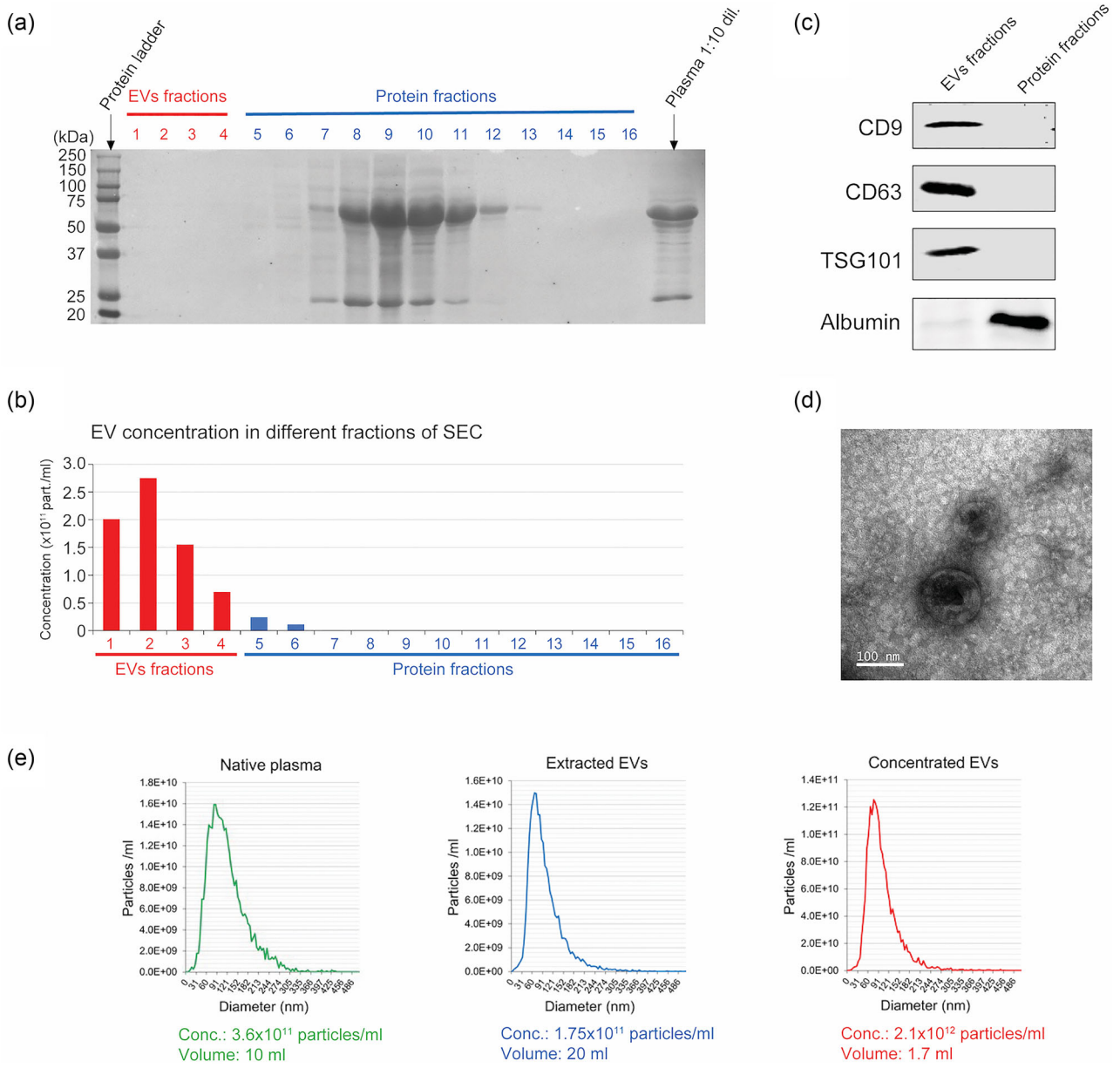

FIGURE 2 Extraction of EVs from mouse plasma. (a) Ponceau S staining of the different plasma fractions after extraction of EVs from mouse plasma by SEC. (b) Nanoparticle tracking analysis of EVs in different plasma fractions (as shown in a) after extraction of EVs by the SEC. (c) Western blot analysis of EV-specific protein markers. Equal amount of total protein was loaded for combined EVs fractions (#1–4), and protein fractions #8–11 (as shown in a). (d) Electron microscopy analysis for the extracted EVs. Scale bar = 100 nm. (e) Nanoparticle tracking analysis of EVs in the native plasma, after extraction from plasma by the SEC (extracted EVs), and after concentration step (concentrated EVs). EVs, extracellular vesicles; SEC, size exclusion chromatography.

incubation at a dose of 5 μg/mL for 2 h. This regimen significantly reduced GP-EVs uptake without affecting the cell cycle of AML-12 cell line. Preincubation of GP-EVs and AML-12 cells with heparin prevented the inhibition of proliferation by total plasma EVs (Figure 3d–g). Unlike GP-EVs, incubation of AML-12 cells with NH-EVs did not affect the cell cycle activity and expression of the proliferation biomarkers (Figure 3d–g). This data indicates that HD-EVs are responsible for the suppression of mouse hepatocyte proliferation in vitro.

To determine the role of RNA carried by HD-EVs in the regulation of hepatocyte proliferation, total RNA (including miRNAs) was extracted from GP-EVs and HD-EVs immunoprecipitated with anti-ASGR1 antibodies. AML-12 cells were transfected with RNA extracted from EVs 24 h after plating. Forty-eight hours after transfection, cells were analyzed for cell cycle distribution and expression of proliferation biomarkers Cyclin D1 and PCNA. Transfection with RNA isolated from GP-EVs caused a dose-dependent arrest in the G1 phase of AML-12 cells (Figure 4a,b), which was accompanied by a significant decrease in the expression

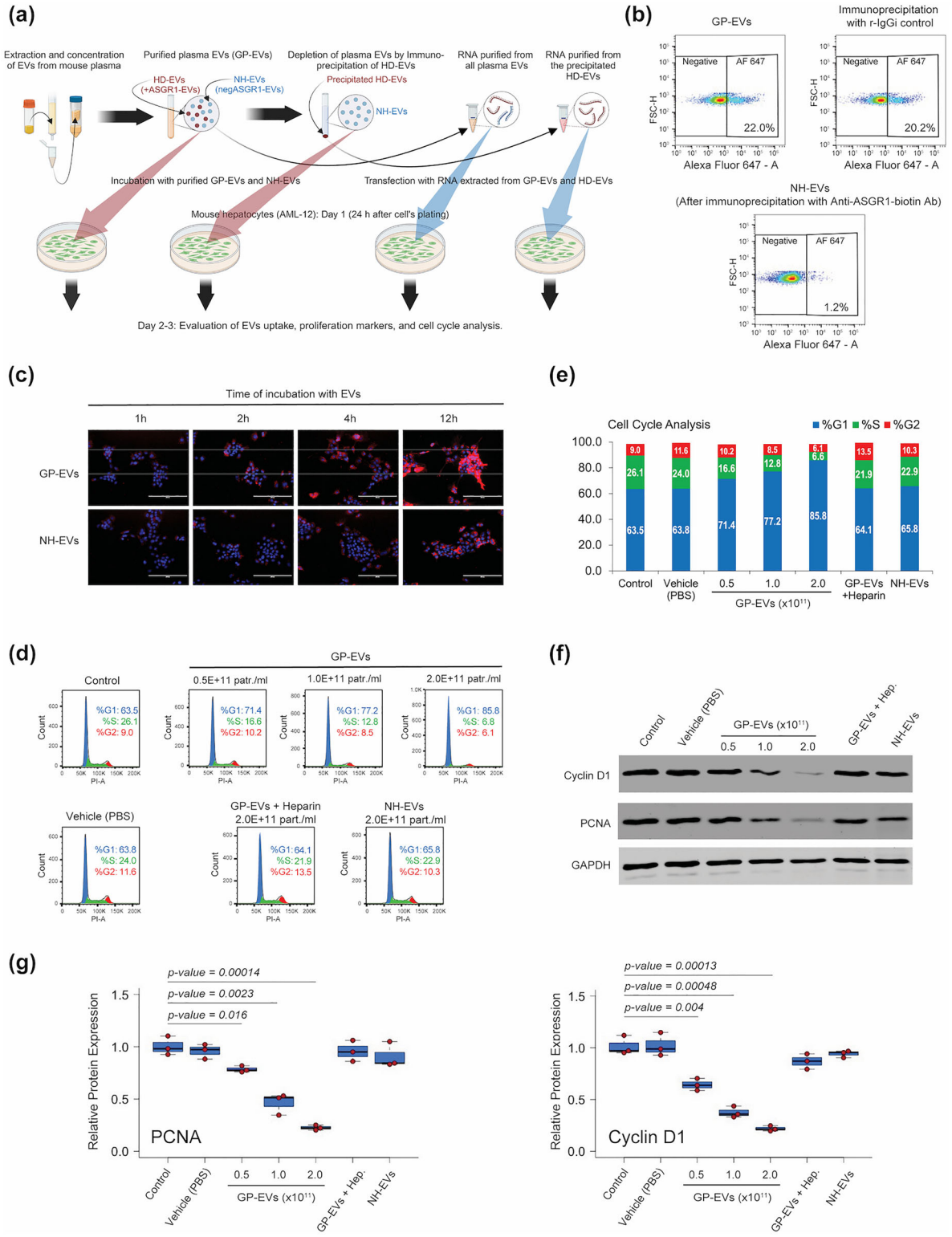

FIGURE 3 HD-EVs blocks proliferation of mouse hepatocytes (AML-12) in vitro. (a) The schematic illustration of the in vitro experiments. (b) Flow cytometry analysis for EVs double-labeled with DiB/AF647-conjugated Anti-mASGR1 in the GP-EVs, after immunoprecipitation with biotinylated Anti-ASGR1 Ab (NH-EVs), and after immunoprecipitation with biotinylated rabbit IgG isotype (r-IgGi) control. (c) EVs uptake assay for the GP-EVs and for the NH-EVs. Twenty-four hours after seeding, AML-12 cells were incubated for different periods of time with two different types of DiL-labelled EVs at a final concentration of 2×10^{11} particles/mL. At the end of the incubation time, the cells were washed, fixed, and stained with mounting media with DAPI. Scale bar = 200 μm. (d) Cell cycle analysis for AML-12 cells incubated with vehicle (PBS) and with different concentrations of GP-EVs extracted from mouse plasma. As negative controls: (i) AML-12 cells and GP-EVs were preincubated for 2 h with 5 μg/mL of Heparin; (ii) AML-12 cells were incubated with NH-EVs. (e) Graph representation of the cell cycle analysis shown in (d). (f) Western blot analysis for expression of Cyclin D1, PCNA, and GAPDH in lysates of AML-12 cells treated as shown in (d). Shown is representative data from three independent experiments. (g) Graphs with quantification of the Western blot analysis as shown in (f). $n = 3$ independent experiments. EVs, extracellular vesicles; GP-EVs, global plasma EVs; NH-EVs, non-hepatocyte EVs; PBS, phosphate-buffered saline.

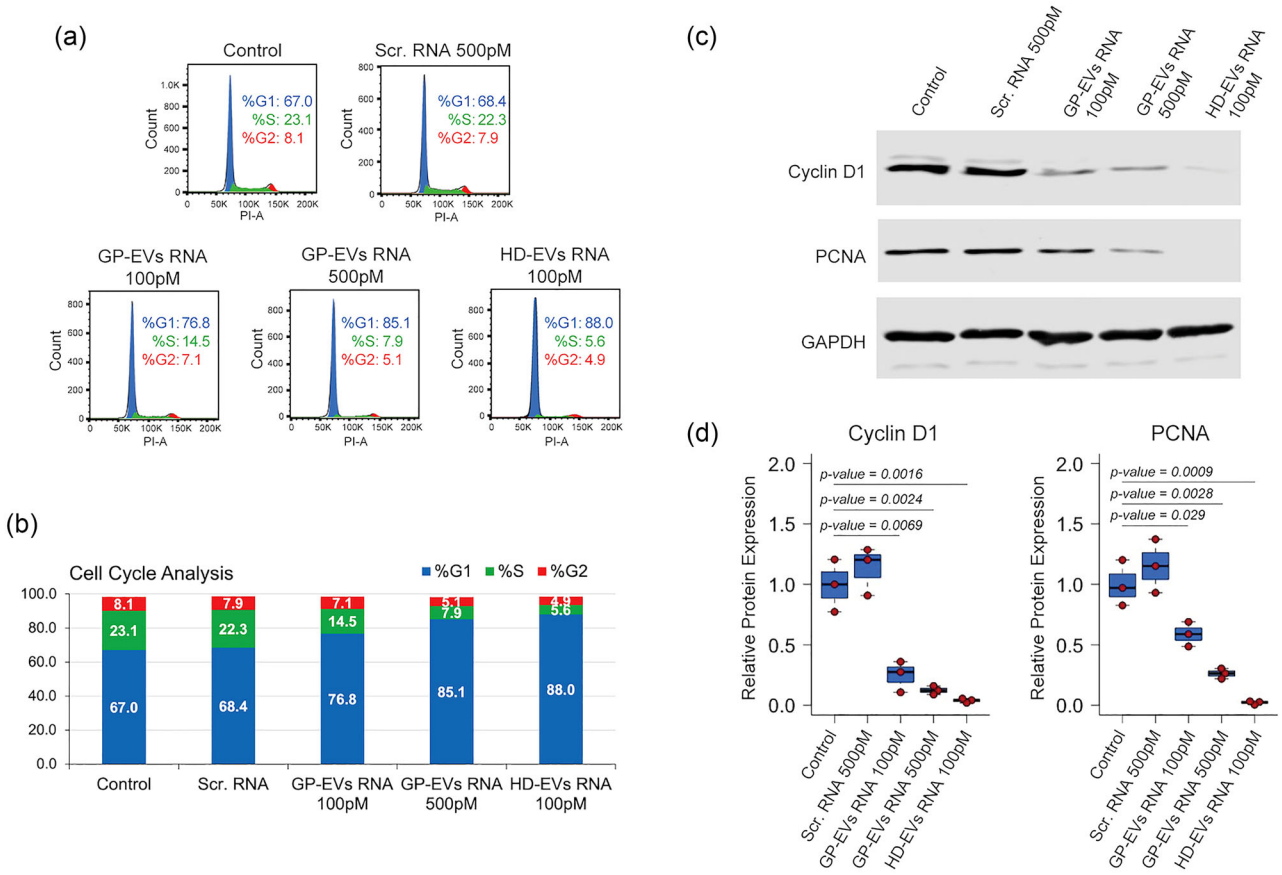

FIGURE 4 RNA extracted from HD-EVs blocks proliferation of mouse hepatocytes (AML-12) in vitro. (a) Cell cycle analysis for AML-12 cells transfected with RNA extracted from GP-EVs, HD-EVs (ASGR1+ EVs), or with negative control siRNA. (b) Graph representation of the cell cycle analysis shown in (a). (c) Western blot analysis for expression of Cyclin D1, PCNA, and GAPDH in lysates of AML-12 cells transfected as shown in (a). Shown is representative data from three independent experiments. (d) Graph with quantification of the Western blot analysis as shown in (c). $n = 3$ independent experiments. EVs, extracellular vesicles; HD-EVs, hepatocyte-derived EVs.

of Cyclin D1 and PCNA proteins (Figure 4c,d). Transfection with RNA isolated from HD-EVs demonstrated a more potent block of AML-12 proliferation compared to RNA from GP-EVs; the effect of 100 pM of HD-EVs-extracted RNA on AML-12 proliferation was more pronounced than the effect of 500 pM of the total EVs-derived RNA (Figure 4a–d).

To evaluate the effect of EVs and RNA they carry on proliferation of hepatocytes in vivo, we used the two-thirds PHx mouse model (Figure 5a). DiR-stained GP-EVs were detected in different organs of mice soon after intravenous (IV) injection (data are not shown); however, 24 h later, a strong signal was only detected in the liver (Figure 5b). After conducting PHx, animals received two sequential IV injections (12 and 24 h post-surgery) with either vehicle (PBS), GP-EVs, or NH-EVs. Thirty-six hours after PHx animals were euthanized, and liver samples were examined by IHC and Western blot analyses (Figure 5c–e). Injection with GP-EVs significantly attenuated PHx-stimulated increase in the expression of Cyclin D1 and PCNA in a mouse liver. Unlike GP-EVs, IV injections with NH-EVs had minimal impact on the expression of Cyclin D1 and PCNA in liver tissue after PHx.

For in vivo transfection with RNA of the remaining lobes of mouse liver after PHx, we used the lipid nanoparticle reagent Invivofectamine 3.0. IV injection of Cy3-labeled Negative Control siRNA in complex with Invivofectamine 3.0 demonstrated that, 48 h post-injection, most of the Cy3-labeled RNA accumulated in liver tissue (Figure 6a). Some accumulation of Cy3-labeled RNA was also observed in the spleen. IV injection of siRNA targeting mRNA for Factor VII in complex with Invivofectamine 3.0 reagent showed that protein expression in liver tissue can be effectively blocked by RNA doses as small as 0.3 mg/kg (Supplemental data, Figure S2), with effects lasting for several days. To test the effect of RNA from HD-EVs on liver regeneration, we conducted an IV injection of HD-EVs-extracted RNA/Invivofectamine 3.0 complex 6 h post-PHx. Forty-eight hours after PHx, IHC, and Western blot analyses demonstrated that in vivo transfection with HD-EVs-extracted RNA significantly attenuated the PHx-stimulated increase in the expression of proliferation biomarkers Cyclin D1 and PCNA in liver tissue (Figure 6b–d). In vivo transfection with the negative control RNA (Scr. RNA) did not affect increase of proliferation markers Cyclin D1 and PCNA

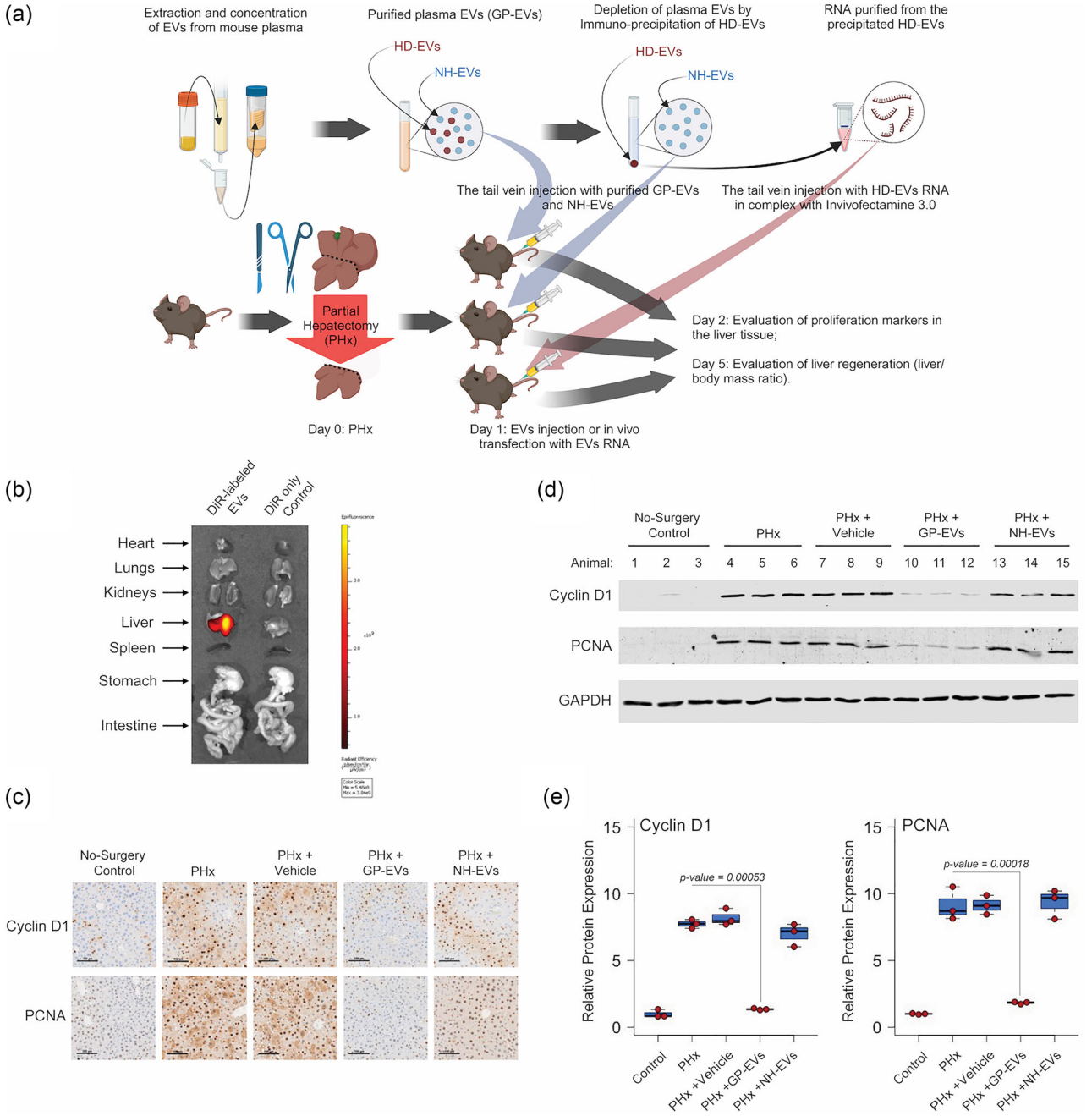

FIGURE 5 HD-EVs blocks proliferation of mouse hepatocytes in vivo after PHx. (a) The schematic illustration of the in vivo experiments. (b) Imaging of the indicated organs for detection of DiR-labelled EVs, 24 h after IV injection of mice with DiR control only and with DiR-labelled GP-EVs (2×10^{11} particles in 200 μL of PBS). (c) IHC for proliferation markers PCNA and Cyclin D1 in mouse liver 36 h after PHx. After PHx, different groups of animals received two IV injections (12 and 24 h after PHx) with: (i) Vehicle (200 μL of PBS) ($n = 3$); (ii) GP-EVs (1×10^{12} particles in 200 μL of PBS) ($n = 3$); (iii) ASGR1-neg EVs (1×10^{12} particles in 200 μL of PBS) ($n = 3$). As a positive control, animals did not receive any IV injections after PHx ($n = 3$). As a negative control, intact animals were used ($n = 3$). Scale bar = 100 μm. (d) Western blot analysis of liver tissue lysates with Cyclin D1, PCNA, and GAPDH for animal groups showed on (c). (e) Graph with quantification of the Western blot analysis as shown in (d). $n = 3$ animals in each group. EVs, extracellular vesicles; HD-EVs, hepatocyte-derived EVs; IHC, immunohistochemistry; PHx, partial hepatectomy

post-PHx. In additional studies, we assessed liver regeneration by calculating the liver-to-body weight ratio 5 days after PHx. Animals that received an IV injection of HD-EVs-extracted RNA/Invivofectamine 3.0 complex 6 h after PHx demonstrated significantly lower liver-to-body weight ratio compared to animals with no injections after PHx (Figure 6e,f). There was no substantial difference in the liver-to-body weight ratio at day 5 after PHx between the animals that received an injection of the negative control RNA/Invivofectamine 3.0 complex and control animals with no injections after PHx.

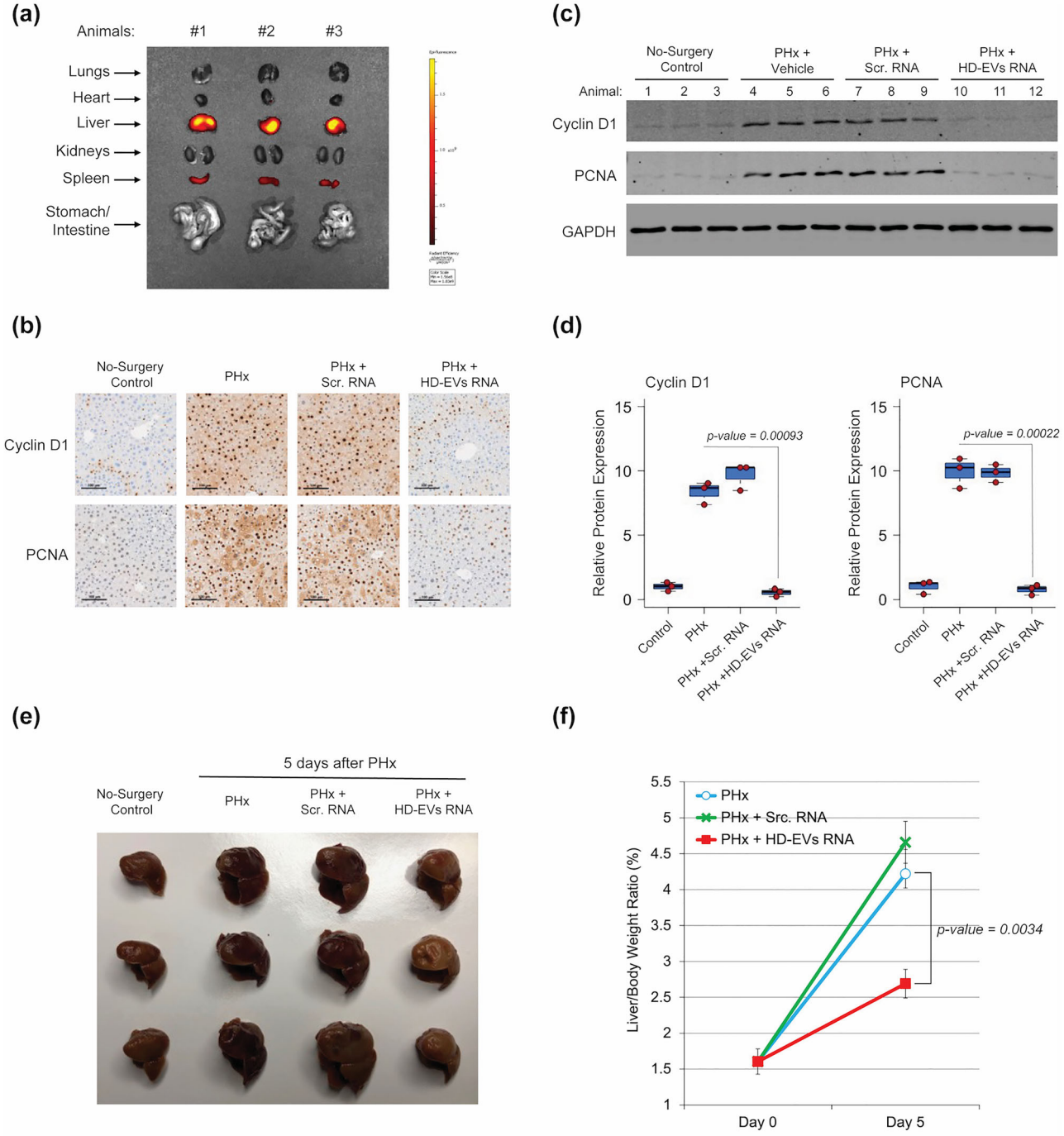

FIGURE 6 RNA extracted from HD-EVs blocks proliferation of mouse hepatocytes in vivo after PHx. (a) Imaging of the indicated organs for detection of Cy3-labeled Negative Control siRNA, 48 h after IV injection in the complex with Invivofectamine 3.0 Reagent. (b) IHC for proliferation markers PCNA and Cyclin D1 in mouse liver 48 h after PHx. Six hours after PHx, different groups of animals were IV injected with Invivofectamine 3.0 Reagent in complex with: (i) 1 mg/kg dose of the Negative Control siRNA ($n = 3$); (ii) 1 mg/kg dose of the RNA extracted from HD-EVs ($n = 3$). As a positive control, animals did not receive any IV injections after PHx ($n = 3$). As a negative control, intact animals were used ($n = 3$). Scale bar = 100 μm. (c) Western blot analysis of liver tissue lysates with Cyclin D1, PCNA, and GAPDH for animal groups showed on (b). (d) Graph with quantification of the Western blot analysis shown in (c). $n = 3$ animals in each group. (e) The median and the right lateral lobes 5 days after PHx from three different groups of animals: (i) no additional treatment; (ii) animals received IV injection of 1 mg/kg dose of the Negative Control siRNA in complex with Invivofectamine 3.0 Reagent, 6 h after PHx ($n = 3$); (iii) animals received IV injection of 1 mg/kg dose of the RNA extracted from HD-EVs in complex with Invivofectamine 3.0 Reagent, 6 h after PHx ($n = 3$). The median and the right lateral lobes of the intact animals (no surgery control) are shown as a negative control. (f) Graph of the quantitative change in the liver/body weight ratio 5 days after surgery for the groups of animals shown in (g). $n = 3$ animals in each group. EVs, extracellular vesicles; HD-EVs, hepatocyte-derived EVs; IHC, immunohistochemistry; PHx, partial hepatectomy.

4 | DISCUSSION

Many studies have focused on the identification of putative inhibitors of liver cell proliferation (ILCP) and the regulation of liver regeneration (Deschamps & Verly, 1975; Iype & McMahon, 1984; Nadal et al., 1976; Saetren, 1956; Sekas et al., 1979; Simard et al., 1974; Verly, 1973). The detection and characterization of ILCP would enable an understanding of the negative feedback mechanism regulating hepatocyte cell cycle initiation, progression, and completion after massive liver tissue loss or injury. Although various fractions of plasma or liver extracts have demonstrated a clear inhibitory effect on hepatocyte proliferation, all attempts to isolate and identify the ILCP responsible for this effect have been unsuccessful. EVs are nanosized, membrane-limited structures secreted by cells into the extracellular space (Tkach & Thery, 2016; van Niel et al., 2018). EVs carry different proteins, lipids, DNA, and RNA. EVs offer a novel mode of cell-to-cell communication, wherein their cargo is transferred from a donor to a recipient cell, leading to alterations in gene expression and cellular function (Buzas, 2023; Grange & Bussolati, 2022; O'Brien et al., 2020; van Niel et al., 2022). Here we show that HD-EVs satisfy most of the previously formulated principal characteristics of ILCP: (a) HD-EVs inhibit mitosis of hepatocytes both in vitro and in vivo; (b) the action of HD-EVs is dose-dependent, reversible, and are not cytotoxic; (c) HD-EVs are synthesized by mature liver hepatocytes upon which they act, and circulate in the blood stream; (d) HD-EVs are tissue-specific: they are taken up by hepatocytes at a much higher rate than EVs from other sources. We demonstrated that the decrease in the concentration of HD-EVs in the blood after PHx correlates with the pronounced and coordinated activation of proliferation of almost all hepatocytes in the remaining lobes of the liver. When the liver mass reaches the initial liver-to-body mass ratio, the plasma HD-EV concentration also reaches the pre-PHx level, leading to the blocking of hepatocyte proliferation and completion of liver regeneration. Restoration of the initial concentration of HD-EV in the blood by IV injection in the post-PHx period blocks the proliferative activity of hepatocytes and significantly slows down liver regeneration. HD-EVs exhibit the same dose-dependent effect in vitro, blocking the proliferation of mouse hepatocytes. It was also shown that RNA isolated from HD-EVs exhibits the same inhibitory effect on hepatocyte proliferation as native HD-EVs. Thus, RNA carried by HD-EVs is an essential component of the mechanism of hepatocyte proliferation inhibition by HD-EVs. Sequence analysis of total RNA extracted from exosomes showed that a diverse collection of the RNA species among which micro-RNAs (miRNAs) were the most abundant, making up over 76.20% of all mappable reads compared to only 1.36% of mRNA coding sequences (Huang et al., 2013). MiRNAs are small (22–24 nucleotides), non-coding RNAs that regulate gene expression at the post-transcriptional level and are the primary regulators of virtually all cellular processes. MiRNAs bind to complementary sequences in the 3′-untranslated region (3′UTR) of target mRNAs, leading to either translational repression or target degradation of the specific mRNA (Bartel, 2009). It is noteworthy that EVs from different cell types carry specific subsets of miRNAs (Jeppesen et al., 2019). MiRNAs have different sorting sequences that determine their packaging into EVs (EXO-motifs) or retention in cells (CELL-motifs), and different cell types preferentially use certain sorting sequences, thereby determining the miRNA profile in EVs for a specific cell type (Garcia-Martin et al., 2022). Thus, we suggest that HD-EVs carry a group of miRNAs, which, when returned to hepatocytes, can suppress the activity of the target genes responsible for cell proliferation. Our next goal is to identify HD-EVs' miRNAs with ILCP activity and their target genes in hepatocytes. There is a possibility that the PHx leads not only to a decrease in the concentration of HD-EVs in the blood but also to a change in their cargo. Thus, the miRNA (and not only miRNA) signature of HD-EVs before and after PHx may be different. In the future, it is necessary to conduct a deep analysis of the content of GP-EVs, HD-EVs, and NH-EVs in different time-points after PHx.

Ying et al. recently demonstrated that liver tissue EVs (LT-EVs) can stimulate the liver regeneration process after PHx and that hepatocytes are the primary source of the LT-EVs in the regenerating liver (Ying et al., 2024). The results of this and our studies indicate that hepatocytes may secrete at least two different types of HD-EVs: the first secreted into the liver tissue and the second secreted into the bloodstream. It seems that these types of HD-EVs are responsible for different functions and should have different cargos. It is obvious that, like any positive feedback mechanism, the mechanism described by Ying et al. for LT-EVs is not able to regulate the cessation of liver cell proliferation when the initial liver/body mass ratio is reached, and further proliferation is not needed. Although the positive feedback mechanism may have a supporting effect on the regenerating liver, it is clear that accurate liver regeneration can only be achieved by a negative feedback mechanism that includes external factors, that is, factors not located in the liver tissue, but secreted by liver cells into the bloodstream.

Our study allows us to conclude that the default state of liver hepatocytes is not rest, but proliferation. Constantly ready for proliferation, hepatocytes are held in the G1 phase of the cell cycle by HD-EVs secreted into the blood and recaptured by hepatocytes. When, due to massive loss or injury to liver tissue, the number of functional hepatocytes sharply decreases, the concentration of HD-EVs in the blood drops below a certain threshold, removing the proliferative block from the remaining hepatocytes, which then synchronously enter the cell cycle. Hepatocyte proliferation continues until the initial number of hepatocytes is restored, and, as a result, the concentration of HD-EVs released by them in the blood reaches the level that blocks further proliferation. It is also possible that a similar EVs-based negative feedback mechanism is responsible for the homeostasis of other constantly renewing tissues.

AUTHOR CONTRIBUTIONS

Mina McGinn: Data curation (supporting); investigation (equal); validation (supporting). **Christopher Rabender**: Formal analysis (equal); investigation (equal); validation (equal); writing—review and editing (equal). **Ross Mikkelsen**: Data curation (equal); formal analysis (equal); investigation (equal); validation (equal); writing—review and editing (equal). **Vasily Yakovlev**: Conceptualization (lead); data curation (lead); funding acquisition (lead); investigation (lead); methodology (lead); project administration (lead); resources (lead); supervision (lead); validation (lead); visualization (lead); writing—original draft (lead).

ACKNOWLEDGEMENTS

TEM and Nanoparticle Tracking Analysis were performed at the VCU Microscopy Facility. Flow Cytometry of the labled EVs was performed at the VCU Flow Cytometry Shared Resource. IVIS analysis was performed at VCU Cancer Mouse Models Core Laboratory. IHC was performed by the Tissue and Data Acquisition and Analysis Core of VCU Massey Comprehensive Cancer Center. All these services are supported, in part, by funding from NIH-NCI Cancer Center Support Grant P30 CA016059. Dr. Yakovlev and Dr. Rabender were supported by the internal fund of the VCU Massey Cancer Center. Figures 3a and 5a were created with BioRender.com.

CONFLICT OF INTEREST STATEMENT

The authors declare no conflicts of interest.

DATA AVAILABILITY STATEMENT

The datasets generated and/or analysed during the current study are available from the corresponding author upon reasonable request.

ORCID

Vasily Yakovlev https://orcid.org/0000-0002-1298-0232

REFERENCES

Apte, U., Gkretsi, V., Bowen, W. C., Mars, W. M., Luo, J. H., Donthamsetty, S., Orr, A., Monga, S. P., Wu, C., & Michalopoulos, G. K. (2009). Enhanced liver regeneration following changes induced by hepatocyte-specific genetic ablation of integrin-linked kinase. *Hepatology*, *50*, 844–851.

Bartel, D. P. (2009). MicroRNAs: Target recognition and regulatory functions. *Cell*, *136*, 215–233.

Bullough, W. S. (1962). The control of mitotic activity in adult mammalian tissues. *Biological Reviews of the Cambridge Philosophical Society*, *37*, 307–342.

Bullough, W. S., & Laurence, E. B. (1960). The control of epidermal mitotic activity in the mouse. *Proceedings of the Royal Society of London. Series B: Biological Sciences*, *151*, 517–536.

Bullough, W. S., & Laurence, E. B. (1968). Epidermal chalone and mitotic control in the Vx2 epidermal tumour. *Nature*, *220*, 134–135.

Buzas, E. I. (2023). The roles of extracellular vesicles in the immune system. *Nature Reviews Immunology*, *23*, 236–250.

Deschamps, Y., & Verly, W. G. (1975). The hepatic chalone. II. Chemical and biological properties of the rabbit liver chalone. *Biomedicine*, *22*, 195–208.

Elgjo, K., & Hennings, H. (1971). Epidermal chalone and cell proliferation in a transplantable squamous cell carcinoma in hamsters. I. in vivo results. *Virchows Archiv B: Cell Pathology*, *7*, 1–7.

Fausto, N., Campbell, J. S., & Riehle, K. J. (2006). Liver regeneration. *Hepatology*, *43*, S45–53.

Garcia-Martin, R., Wang, G., Brandao, B. B., Zanotto, T. M., Shah, S., Kumar Patel, S., Schilling, B., & Kahn, C. R. (2022). MicroRNA sequence codes for small extracellular vesicle release and cellular retention. *Nature*, *601*, 446–451.

Grange, C., & Bussolati, B. (2022). Extracellular vesicles in kidney disease. *Nature Reviews Nephrology*, *18*, 499–513.

Huang, X., Yuan, T., Tschannen, M., Sun, Z., Jacob, H., Du, M., Liang, M., Dittmar, R. L., Liu, Y., Liang, M., Kohli, M., Thibodeau, S. N., Boardman, L., & Wang, L. (2013). Characterization of human plasma-derived exosomal RNAs by deep sequencing. *BMC Genomics*, *14*, 319.

Iversen, O. H. (1968). Effect of epidermal chalone on human epidermal mitotic activity in vitro. *Nature*, *219*, 75.

Iype, P. T., & McMahon, J. B. (1984). Hepatic proliferation inhibitor. *Molecular and Cellular Biochemistry*, *59*, 57–80.

Jeppesen, D. K., Fenix, A. M., Franklin, J. L., Higginbotham, J. N., Zhang, Q., Zimmerman, L. J., Liebler, D. C., Ping, J., Liu, Q., Evans, R., Fissell, W. H., Patton, J. G., Rome, L. H., Burnette, D. T., & Coffey, R. J. (2019). Reassessment of exosome composition. *Cell*, *177*, 428–445e418.

Jirtle, R. L., & Michalopoulos, G. (1982). Effects of partial hepatectomy on transplanted hepatocytes. *Cancer Research*, *42*, 3000–3004.

Jung, M. K., & Mun, J. Y. (2018). Sample preparation and imaging of exosomes by transmission electron microscopy. *Journal of Visualized Experiments: JoVE*, *131*, e56482.

Laird, A. K. (1965). Dynamics of tumour growth: Comparison of growth rates and extrapolation of growth curve to one cell. *British Journal of Cancer*, *19*, 278–291.

Laurence, E. B., & Elgjo, K. (1971). Epidermal chalone and cell proliferation in a transplantable squamous cell carcinoma in hamsters. II. in vitro results. *Virchows Archiv B: Cell Pathology*, *7*, 8–15.

Leong, G. F., Grisham, J. W., Hole, B. V., & Albright, M. L. (1964). Effect of partial hepatectomy on DNA synthesis and mitosis in heterotopic partial autografts of rat liver. *Cancer Research*, *24*, 1496–1501.

Marrs, J. M., & Voorhees, J. J. (1971). Preliminary characterization of an epidermal chalone-like inhibitor. *Journal of Investigative Dermatology*, *56*, 353–358.

Maugh, T. H. 2nd (1972). Chalones: chemical regulation of cell division. *Science*, *176*, 1407–1408.

Michalopoulos, G. K., & Bhushan, B. (2021). Liver regeneration: biological and pathological mechanisms and implications. *Nature Reviews Gastroenterology & Hepatology*, *18*, 40–55.

Michalopoulos, G. K., & DeFrances, M. C. (1997). Liver regeneration. *Science*, *276*, 60–66.

Mitchell, C., & Willenbring, H. (2008). A reproducible and well-tolerated method for 2/3 partial hepatectomy in mice. *Nature Protocols*, *3*, 1167–1170.

Moolten, F. L., & Bucher, N. L. (1967). Regeneration of rat liver: transfer of humoral agent by cross circulation. *Science*, *158*, 272–274.

Nadal, C., Lombard, M. N., & Zajdela, F. (1976). Inhibition of rat hepatocyte multiplication by serum and liver factors: physiological development and experimental induction. *Virchows Archiv B: Cell Pathology*, *20*, 277–285.

Nome, O. (1975). Tissue specificity of the epidermal chalones. *Virchows Archiv B: Cell Pathology*, *19*, 1–25.

O'Brien, K., Breyne, K., Ughetto, S., Laurent, L. C., & Breakefield, X. O. (2020). RNA delivery by extracellular vesicles in mammalian cells and its applications. *Nature Reviews Molecular Cell Biology*, *21*, 585–606.

Povero, D., Yamashita, H., Ren, W., Subramanian, M. G., Myers, R. P., Eguchi, A., Simonetto, D. A., Goodman, Z. D., Harrison, S. A., Sanyal, A. J., Bosch, J., & Feldstein, A. E. (2020). Characterization and proteome of circulating extracellular vesicles as potential biomarkers for NASH. *Hepatology Communications*, *4*, 1263–1278.

Rodrigues, A. D., van Dyk, M., Sorich, M. J., Fahmy, A., Useckaite, Z., Newman, L. A., Kapetas, A. J., Mounzer, R., Wood, L. S., Johnson, J. G., & Rowland, A. (2021). Exploring the use of serum-derived small extracellular vesicles as liquid biopsy to study the induction of hepatic cytochromes P450 and organic anion transporting polypeptides. *Clinical Pharmacology & Therapeutics*, *110*, 248–258.

Saetren, H. (1956). A principle of auto-regulation of growth; production of organ specific mitose-inhibitors in kidney and liver. *Experimental Cell Research*, *11*, 229–232.

Sekas, G., Owen, W. G., & Cook, R. T. (1979). Fractionation and preliminary characterization of a low molecular weight bovine hepatic inhibitor of DNA synthesis in regenerating rat liver. *Experimental Cell Research*, *122*, 47–54.

Simard, A., Corneille, L., Deschamps, Y., & Verly, W. G. (1974). Inhibition of cell proliferation in the livers of hepatectomized rats by a rabbit hepatic chalone. *PNAS*, *71*, 1763–1766.

Starzl, T. E., Fung, J., Tzakis, A., Todo, S., Demetris, A. J., Marino, I. R., Doyle, H., Zeevi, A., Warty, V., & Michaels, M. (1993). Baboon-to-human liver transplantation. *Lancet*, *341*, 65–71.

Thery, C., Amigorena, S., Raposo, G., & Clayton, A. (2006). Isolation and characterization of exosomes from cell culture supernatants and biological fluids. *Current Protocols in Cell Biology*, Chapter 3:1, p. 3–22.

Tkach, M., & Thery, C. (2016). Communication by extracellular vesicles: Where we are and where we need to go. *Cell*, *164*, 1226–1232.

van Niel, G., Carter, D. R. F., Clayton, A., Lambert, D. W., Raposo, G., & Vader, P. (2022). Challenges and directions in studying cell-cell communication by extracellular vesicles. *Nature Reviews Molecular Cell Biology*, *23*, 369–382.

van Niel, G., D'Angelo, G., & Raposo, G. (2018). Shedding light on the cell biology of extracellular vesicles. *Nature Reviews Molecular Cell Biology*, *19*, 213–228.

Verly, W. G. (1973). The hepatic chalone. *National Cancer Institute Monograph*, *38*, 175–184.

Weiss, P., & Kavanau, J. L. (1957). A model of growth and growth control in mathematical terms. *Journal of General Physiology*, *41*, 1–47.

Ying, S. Q., Cao, Y., Zhou, Z. K., Luo, X. Y., Zhang, X. H., Shi, K., Qiu, J. Y., Xing, S. J., Li, Y. Y., Zhang, K., Jin, F., Zheng, C. X., Jin, Y., & Sui, B. D. (2024). Hepatocyte-derived tissue extracellular vesicles safeguard liver regeneration and support regenerative therapy. *Journal of Nanobiotechnology*, *22*, 521.

SUPPORTING INFORMATION

Additional supporting information can be found online in the Supporting Information section at the end of this article.

How to cite this article: McGinn, M., Rabender, C., Mikkelsen, R., & Yakovlev, V. (2024). Hepatocyte-derived extracellular vesicles regulate liver regeneration through a negative feedback mechanism. *Journal of Extracellular Biology*, *3*, e70023. https://doi.org/10.1002/jex2.70023